Short term forecasting of solar radiation based on satellite data

Elke Lorenz, Annette Hammer, Detlev Heinemann
Energy and Semiconductor Research Laboratory, Institute of Physics
Carl von Ossietzky University, D-26111 Oldenburg

Forecasting of solar irradiance will become a major issue in the future integration of solar energy resources into existing energy supply structures. Fluctuations of solar irradiance have a significant influence on electric power generation by solar energy systems. An efficient use of solar energy conversion processes has to account for this behaviour with respective operating strategies. Examples are the management of electricity grids with high penetration rates from solar sources and the thermal control of buildings. This paper focusses on forecasting the surface solar irradiance in a short term time range of 30 minutes to 6 hours.
As far as short term horizons are concerned, satellite data are a high quality source for irradiance information because of excellent temporal and spatial resolution. Due to the strong impact of cloudiness on surface irradiance, the description of the temporal development of the cloud situation is essential for irradiance forecasting. As a measure of cloudiness, cloud index images according to the Heliosat method, a semi-empirical methode to derive radiation from satellite data, are calculated from the satellite images. To predict the future cloud index image in a first step motion vector fields are derived from two consecutive images. The future image then is determined by applying the calculated motion vector field to the actual image. Finally, solar surface irradiance is derived from the predicted cloud index images with the Heliosat method. Figure 1 gives an overview of these steps to derive the irradiance forecast.
For an effective application of forecast information, it is important to estimate the uncertainty of the forecast accuratly. The accuracy of the forecasted irradiance depends on the meteorological situation. Thus, it is possible to distinguish different levels of accuracy. It will be shown that there are good results of the forecast for situations with high irradiance, where as it is more difficult to forecast situations with variable cloud cover or low sun elevations. The assessment of the forecast quality was performed for single metoerological stations and for a regional forecast. The first section of this paper gives a brief introduction to the calculation of cloud and radiation maps from satellite data. In the next section the algorithm to forecast cloud index images is described. Finally in the last section a detailed error analysis of the forecast is performed.

Calculation of cloud and radiation maps

Images in the visible range of the geostationary satellite METEOSAT are used as a database for the forecast. The satellite maps the full earth disc every 30 minutes with a spatial resolution of approximately 2.5 km x 3.5 km for central Europe.
The surface irradiance and information on clouds are derived from the satellite measurements using an enhanced version of the semi-empirical Heliosat method (Cano et al., 1986, Hammer et al., 1999).

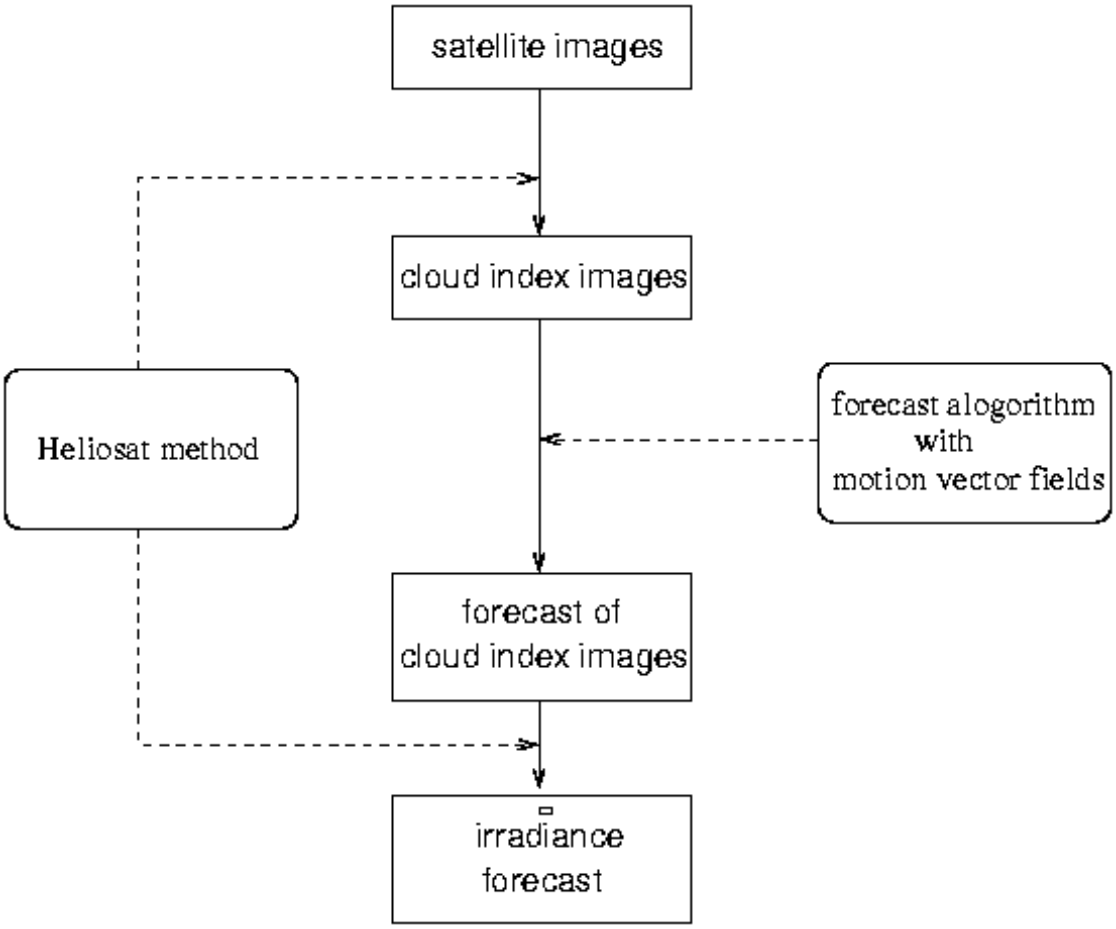

Figure 1: schematic diagram of the forecast routine

The original satellite radiometer count c is reduced by an offset c_0 in a first step to account for the sensor offset and the reduction of the radiation on its way through a cloudfree atmosphere. A relative reflectivity ρ is calculated from this corrected signal by applying a normalisation with respect to the solar zenith angle. In a second step, the cloud index n is derived from the relative reflectivity for each pixel as a dimensionless measure of cloudindess, where the fact, that ground and clouds show different reflectivities, is utilized. The cloud index value determines the contributions of cloud reflected radiation with refelectivity ρ_{cl} and ground reflected radiation with refelctivity ρ_{gr} respectively:

$$\rho = n\rho_{cl} + (1-n)\rho_{gr}. \quad (1)$$

From satellite images the constant cloud reflectivity ρ_{cl} and monthly maps of the ground albedo ρ_{gr} are derived. The cloud index then is calculated using equation (1):

$$n = (\rho - \rho_{gr})/(\rho_{cl} - \rho_{gr}). \quad (2)$$

In the Heliosat method a linear relationship between cloud index n and the atmospheric transmission k^* is assumed with k^* being defined as the ratio beween surface global irradiance G and the clearsky irradiance G_{clear} :

$$k^* = G / G_{clear} = 1 - n. \quad (3)$$

The global irradiance G then can be calculated directly from k^* using a clearsky model to determine $G_{clear.}$

Average errors of satellite retrieved irradiance compared to hourly mean values of ground measurements are 20-25%.

Forecast of cloudindex images

As shown in figure 1 the forecast algorithm is applied to cloud index images.
The advantage of operating on cloud index images instead of irradiance maps is the independency on daily patterns of irradiance. This allows to focus on the development of cloud structures, the deterministic daily variation of irradiance is added through the use of a clear sky model, according to equation (3).
The temporal change of cloud strucures is, for short term scales, mainly caused by cloud motion.
Therefore, motion vector fields were used to forecast cloud index images. This approach is illustrated in figure 2.
Several approaches to derive motion vector fields have been proposed. (Beyer et al. (1994), Bannehr et al. (1994), and Cote and Tatnall (1995)).
The algorithm for detection of motion used within this paper is based on the following model of motion describing the basic assumptions about motion:

- Pixel intensities stay constant during motion.
- The motion vector field is smooth, i.e. neighbouring vecors do not differ a lot in direction and length.

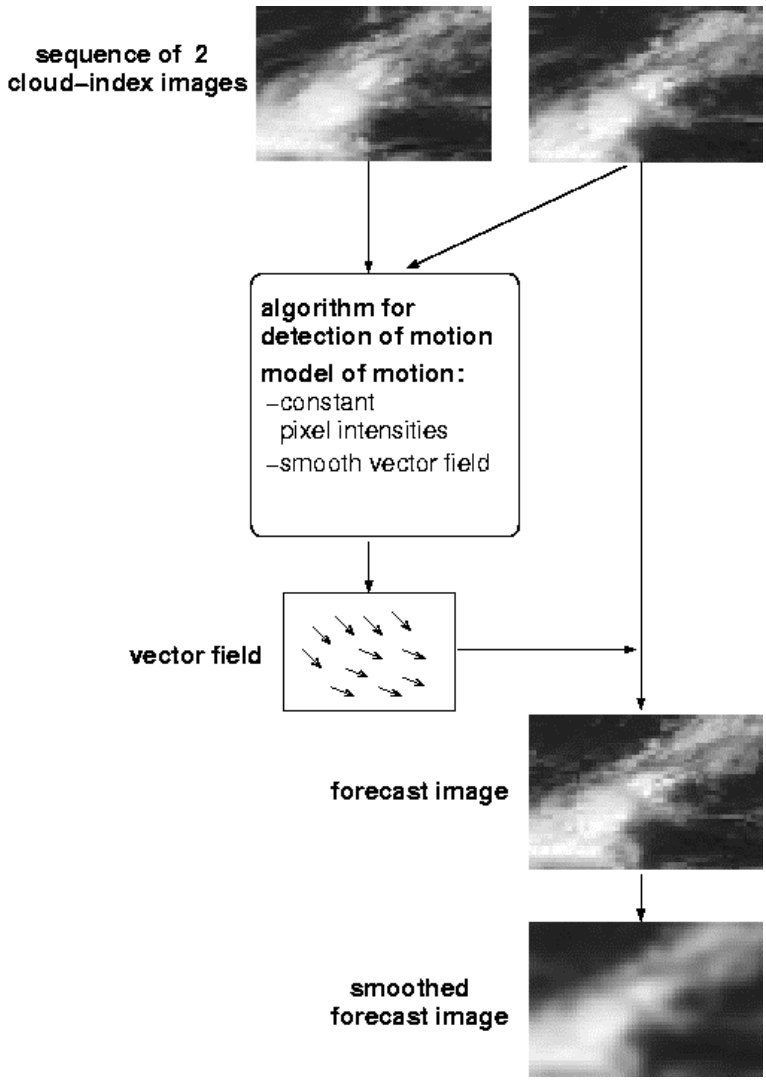

Figure 2: schematic diagram of forecast of cloud index images

The calculated motion vector field is applied to the actual image to derive the forecast image. In a last step a smoothing filter is applied to the forecasted image. Small scale structures vary randomly and their development cannot be predicted. Thus, filtering this 'noise' considerably improves the quality of the forecast.

Motion vector fields

To derive motion vector fields corresponding regions are identified in two consecutive iamges according to the model of motion.
The assumption of constant pixel intensities leads to:

$$n_1(\vec{x}_0 + ((t_1 - t_0)\vec{v}(\vec{x}_0)) \approx n_0(\vec{x}_0), \quad (4)$$

for a vector $\vec{v}$ describing the motion. Here $n_i(\vec{x})$ is the cloud index at position $\vec{x}$ in the image at time t_i. The past image is subscribed with 0, the actual image with 1. As the vector field is

assumed to be smooth, the vector $\vec{v}$ is a good approximation for neighbouring pixels of $\vec{x}_o$ also. Thus,

$$r_i = n_1(\vec{x}_i + (t_1 - t_0)\vec{v}(\vec{x}_i)) - n_0(\vec{x}_i) \quad (5)$$

is small for pixels close to $\vec{x}_o$.

The displacement vecor that minimizes the mean square pixel differences for a rectangular region around $\vec{x}_o$

$$mse = \frac{1}{N}\sum_i r_i^2 \quad (6)$$

is chosen as the vector that describes motion best.

On the one hand side the size of the region to determine the mean square pixel differences should be large enough to contain information on cloud structures. On the other hand the assumption, that the same vector describes the motion for the whole region is better fulfiled for small regions. Best results were achieved for regions with a minimum size of 5 x 30 pixels (90 km x 90 km). Further extension of the regions does not incfluence the forecast quality significantly.

The second parameter, that has to determined to derive the motion vector field, is the resolution of the vector field. The distance between vectors was chosen 25 km, because the improvement for higher resolutions is neglectable.

The derived motion vector fields are applied to the present image n_1 to derive the forecast image n_2. Depending on the forecast horizon the vectors are scaled with the corresponding time difference between present and forecast image:

$$n_2(\vec{x}_0) = n_1(\vec{x}_0 - (t_2 - t_1)\vec{v}(\vec{x}_0)). \quad (7)$$

Smoothing of forecast images

The application of an appropriate smoothing filter on the forecast images significantly improves the forecast quality as stated above. Two different types of smoothing filters where investigated, binomial filters and rectangular filters.

The mean rmse between the original and the forecast images for a time series is considered to evaluate the forecast quality. For comparison errors of persistence are calculated, where persistence means that the actual image is

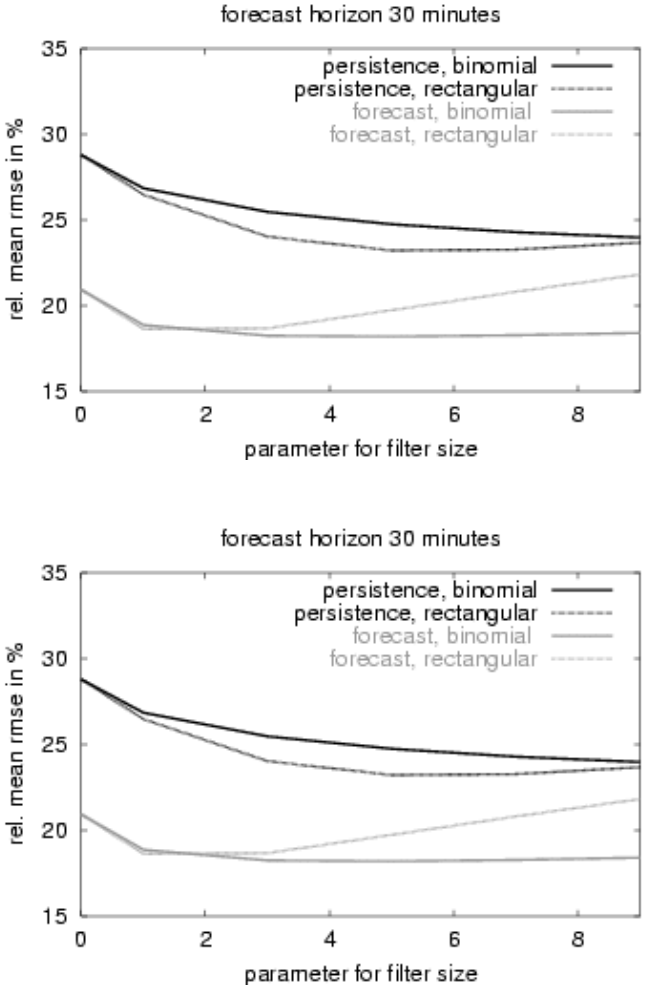

Figure 3: relativ mean rmse of forecast of cloud index values depending on the filter size of the smoothing filter. Comparison of rectangular and binominal filters for persistence and forecast. upper picture: forecast horizon 30 minutes lower picure: forecast horizon 2 hours

taken as the forecast:

$$n_2(\vec{x}_0) = n_1(\vec{x}_0). \quad (8)$$

The results for the two filter types depending on the filter size are displayed in figure 3 for the forecast horizon of 30 minutes and 2 hours.
The forecast shows considerably smaller errors than persistence for both forecast horizons. Furthermore, figure 3 illustrates the significant reduction of forecast errors by appliance of moothing filters. The optimum filter size is increasing with increasing forecast horizon. For a forecast horizon 30 minutes the optimum filter size for the forecast with rectangular filters is 3x3 pixels, while for a forecast of horizon of 2 hours a filter size of 30x30 pixel gives best results. Binomial filters lead to slightly better results for a forecast horizon of 30 minutes. For larger forecast horizons, where averaging over a larger area is required to achieve optimum forecast quality, rectangular filters are more suitable.
The evaluation of the forecast quality for cloud index images shows, that the forecast algorithm based on motion vector fields in combination with the application of smoothing filters performs significantly better than persistence.
A second approach to derive motion vector fields on a statistical base (Hammer et al. (2000)) resulted in the same forecast quality.

Quality assessment of irradiance forecast

The forecast of irradiance values is derived from the forecasted cloud index images using the Heliosat method (see figure 1). To evaluate the overall error of the method, the forecast results were compared to half hourly ground measured irradiance values. The quality assessment was performed for single stations and regional forecasts, corresponding to different scales of application. For the management of buildings and stand alone photovoltaic systems point forecasts are required. Large scale applications like grid integration of photovoltaics benefit from area averaged forecasts.
Data (4/1995-3/1996) from a regional measurement network for global radiation in the region of Saarbrücken (Germany) were used for the evaluation. To derive the regional forecasts, average values of 8 stations distributed over an area of 31km x 45km were calculated.
Figure 4 shows the relative rmse of the forecast of gobal irradiance for a single station. For comparison persistence, persistence with application of a smoothing filter, and the forcast without smooting are displayed. As a lower limit of the forecast quality the error of the Heliosat method to derive irradiance from satellite data is given.
As for cloud index values, the forecast algorithm significantly reduces the errors compared to persistence. With increasing forecast horizon the influence of smoothing becomes more important compared to the reduction of errors due to the application of the motion vector

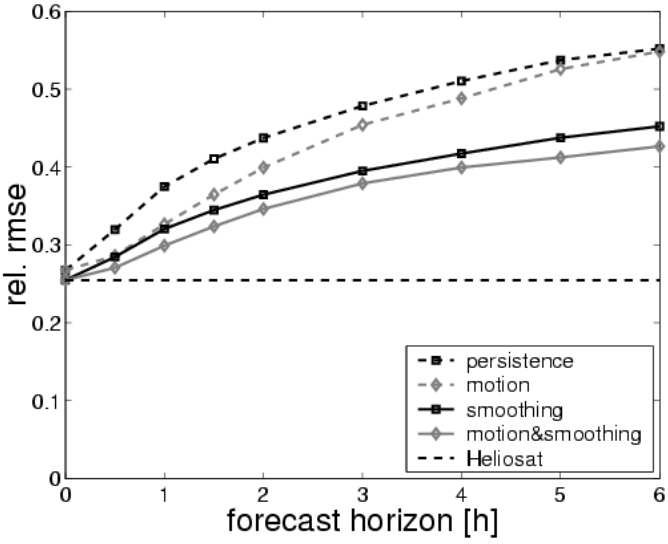

Figure 4: rel. rmse of forecast of global irradiance over the forecast horizon.

fields. Furthermore, figure 4 illustrates that the error of the Heliosat method considerably contributes to the overall forecast error, especially for very short forecast horizons.
An accuarate specification of forecast errors is an important point for an effective application of the forecast. Therefore, a detailed two-dimensional error analysis was performed to distinguish situations of different forecast quality. The detailed error analysis was performed for the clearsky index k* (see equation (5)).
Two parameters were chosen to characterize situations with different levels of accuracy: sun elevation and variability of the cloud index images. For situations with inhomogene clouds, corresponding to a high variability in the cloud index images, forecasting of cloud index images as well as the derivation of ground irradiance from satellite data, are more difficult and larger errors are expected. As a measure of variability a local, spatial variability index is defined:

$$\mathrm{var} = \sqrt{\frac{1}{N}\sum_{i,j}(n_{i+1,j} - n_{i,j})^2 + (n_{i,j+1} - n_{i,j})^2)},$$

where $n_{i,j}$ is the cloud index value at postion i,j in the image, the summation is carried out for a 7x7 pixel region around the pixel corresponding to the ground station, and N is the number of pixels considered.
As a first step of the detailed error analysis the relative standard error of the Helisoat method is displayed over sun elevation and the variability index in figure 5. The accuracy of the Helisoat method shows a clear dependency on both parameters. Forecast errors are increasing drastically for low sun elevations, while for sun elevations higher than 20° the standard error is below 40% for all situations. For sun elevations higher than 20° there is a very high accuracy of the Heliosat method with errors smaller than 10 % for very low variabilities corresponding to clear sky situations. With increasing variability index the accuracy of the satellite derived irradiance is decreasing.

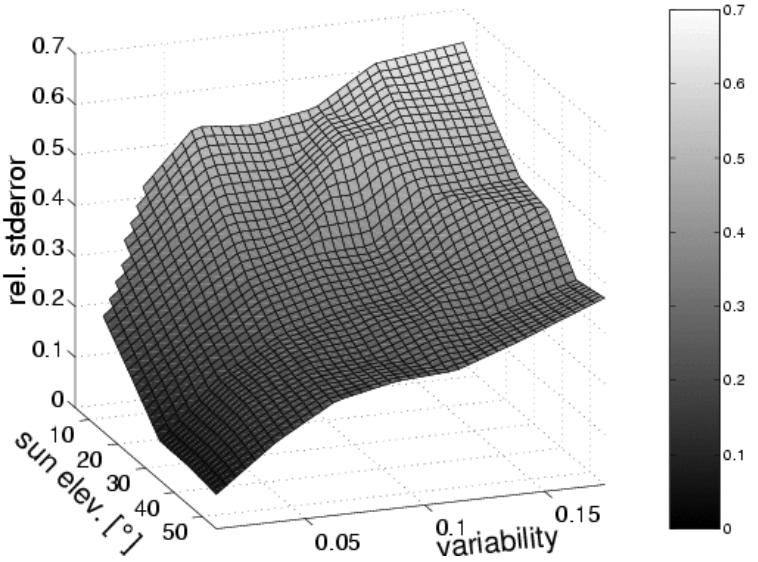

Figure 5: rel. stderror of k for the Heliosat method depending on the sun elevation and the variability.*

To extend the two dimensional error analysis to the forecast, different classes with respect to sun elevation and variability index are defined. For low sun elevations the forecast errors exeed 40% for all forecast horizons. For sun elevations > 20° the relative standard error depending on the forecast horizon for the different variability classes is plotted in figure 6. The upper picture shows the evaluation for a single station. In cases of high irradiance with very low spatial variabilities the error for half hourly irradiance values ranges from 10% for a forecast horizon of 30 minutes to 25% for a forecast horizon of 6 hours. For higher variabilities the forecast errors are considerably higher.
In the lower picture of figure 6 the forecast errors are given for an average regional forecast . The errors are reduced significantly compared to single stations. As for single stations different levels of accuracy are are given for the different variability classes. For low sun elevations the errors of the regional forecast are comparable with the errors of a single station.

To complete the error analysis, forecast errors are compared to persistence of ground derived values of k*and to the standard deviation of the irradiance time series as an upper limit for forecast errors. The corresponding curves for the relative standard error over the forecast horizon are given in figure 7 for the example sun elevation >20^o and 0.025 < var < 0.05. Figure 7 shows that the satellite based forecast as well as persistence of satellite data with application of a smoothing filter performs a lot better than persistence of ground derived values of k*. This result is due to the importance of spatial information on the cloud structure for irradiance forecasting.

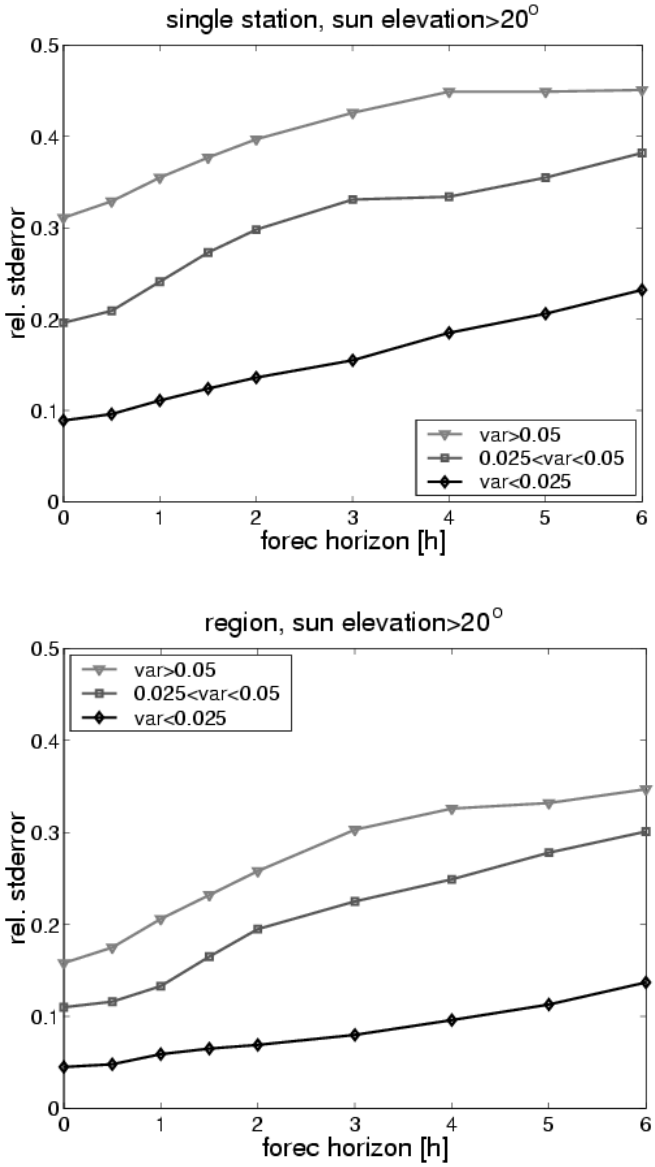

Figure 6: rel stderror of the forecast of k depending on the forecasthorizon for different variability classes and sun elevation>20^o*
upper picure: forecast for a single station
lower picture: forecast for a region of 35kmx45km

Conclusions

A method to predict solar irradiance on the base of satellite data was presented. Motion vector fields are used to forecast cloud index images and smoothing filters are applied on the forecasted images. Evaluation with ground data showed that there is a remarkable improvement in forecast accuracy compared to both satellite and ground derived persistence. For regional forecasts the errors are signficantly lower compared to single stations.
Different levels of accuracy can be distinguished by regarding the parameters sun elevation and spatial variability of the cloud index images. The forecast is very accurate in cases of high irradiance with low spatial varaibility and sun elevations higher than 20^o. Whereas for low sun elevation and high variabilities the error exceeds 40% for all forecast horizons. Further improvements of the irradiance forecast are expected with the development of improved algorithms for the conversion of satellite data to ground irradiance, because the error of the Heliosat method contributes considerably to the overall forecast error. With the introduction of the new satellite generation MSG (Meteosat Second Generation) more accurate algorithms to derive solar irradiance will be available in near future (Müller et al. (2003)).

The presented algorithm to forecast solar irradiance is an appropriate method for short term forecast horizons. Methods to predict irradiance for forecast horizons up to two days on the base of mesoscale weather models are under development.

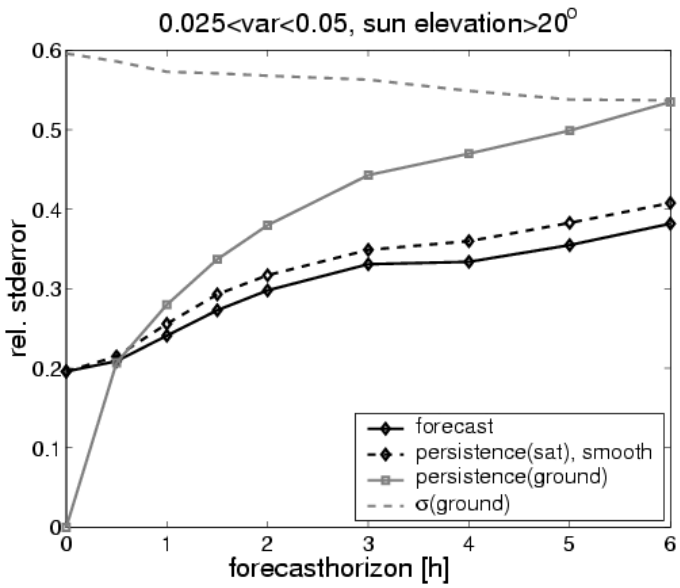

Figure 7: *rel. stderror of the forecast of k* depending on the forecast horizon. Comparison of satellite derived forecast to persistence of ground derived values of k*.*

References

Bahner L., Rohn M., and Warnecke G.(1996). A functional analytic method to derive displacement vector fields from satellite image sequences. *Int. J. Remote Sensing* **17**, pp 383--392

Beyer H.G., Costanzo C., Heinemann D., and Reise C. (1994). Short range forecast of PV energy production using satellite image analysis*. Proceedings of 12th European Photovoltaic Solar Energy Conference*, 11-15 April, Amsterdam, The Netherlands, pp. 1718-1721.

Cano D., Monget J.M. Albussion M., Guillard H., Regas N., and Wald L. (1986). A method for the determination of global solar radiation from meteorological satellite data, *Solar Energy* **37**, pp. 31-39.

Cote S. and Tatnall A.R.L.A (1995). Neural network based method for tracking features from satellite sensor Images*. Int. J. Remote Sensing* **16**, pp. 3695-3701.

Hammer A., Heinemann D., and Westerhellweg A. (1999). Daylight and solar irradiance data derived from satellite observations - The Satellight Project. *Proc. ISES Solar World Congress*. Jerusalem, 1999.

Hammer A., Heinemann D., Lorenz E., and Lueckehe B. (2000) Short- term forecasting of solar radiation: a statistical approach using satellite data. *Solar Energy, **67**,* pp.139—150.

Müller R. W., Heinemann D., Kuhlemann R., Reise C., Dagestad K. F. , Olseth J.A. , Cros S., Wald L., Schroedter M., Dumortier D., Ineichen P., and Piernavieja G. (2003). Rethinking satellite based solar irradiance modelling- The SOLIS clear sky module. Submitted *to Remote Sensing of the Environment*, 2003